A High-Order Cut-Cell Method for Numerical Simulation of Hypersonic-Boundary Transition with Surface Roughness

Le Duan* , Xiaowen Wang † and Xiaolin Zhong.‡
University of California, Los Angeles, California 90095

Hypersonic boundary-layer transition can be effected significantly by surface roughness. In this paper, the receptivity process induced by interaction of Mach 5.92 flow over flat plate under the combination effect of two-dimensional surface roughness and blow-suction is investigated. A new high-order cut-cell method is developed to generate cut cells in the irregular domain. The governing Navier-Stokes equations are solved by using third-order non-uniform upwind finite difference method in the irregular cells. A high-order shock-fitting method is also employed to treat the upper bow-shock to maintain the overall accuracy. Both steady state solutions and unsteady solutions have been obtained by using the new method. For simulating steady flow with roughness, there is significant change inside the boundary layer, but not vary significantly away from the wall. For unsteady flow, the preliminary results for flow instability induced by both blow-suction slot and roughness have also been obtained.

I. Introduction

The mechanism of roughness induced laminar-turbulence transition of boundary layer is important to design hypersonic vehicles. Transition can have a first order influence on their body lift and drag, stability and control and heat transfer property. For example, swept wings are used for most commercial and military aircraft. It has been know that the aerodynamics parameter may vary substantially after transition. Thus to understand the fundamental instability mechanisms in swept-wing flows is crucial considering its board application in aerospace design [1]. Another application of studying roughness induced transition is for the design of thermal heat protection system of hypersonic vehicles. For a reentry vehicle entering earth's atmosphere, it initially experiences a heating environment associated with a laminar boundary layer. Eventually with the attitude decreasing, the vehicle surface become rougher and the boundary layer become turbulent and the heating rate at the surface can be increased by a factor of four or more [2]. Thus the ability to understand and predict the roughness induced transition plays an essential role in thermal protection system (TPS) design process. However, roughness induced laminar-turbulence transition in hypersonic boundary layers is still poorly understood due to the limitation in experimental facilities and numerical methods [4].

Laminar-Turbulence transition process generally consists of three stages. They are receptivity, linear and nonlinear growth of instability waves and breakdown to turbulence. There has been recent development of using transition growth theory as an explanation for by-pass transition due to surface roughness [11]. Within the entire laminar-turbulence transition process, the receptivity process involves the generation and excitation of instability wave (T-S waves) inside the boundary layer under various external environmental perturbations [3]. The receptivity and transition process induced by surface roughness is one of the frequently studied fields in the last decades. The instability mechanisms associated two-dimensional roughness (Spanwise invariant three-dimensional roughness) have been studied since the model behind it is simple in analyzing and simulating both from the theoretical and experimental point of view. There is a conclusion that both of the frequency of external free stream disturbance and surface roughness can affect the amplitude of T-S instable waves [4]. A linear relationship between amplitude of T-S wave and height of roughness can be observed for small roughness in low speed flow [14].

* Graduate Research Assistant, Department of Mechanical&Aerospace Engineering, Member, AIAA
† Research Scientist , Department of Mechanical&Aerospace Engineering, Member, AIAA
‡ Professor, Department of Mechanical&Aerospace Engineering, Associate Fellow, AIAA

There have been extensive theoretical studies on roughness induced receptivity and transition, mainly for incompressible flow. Goldstein [5] developed an asymptotic analysis approach for localized receptivity, utilizing the triple-deck structure. The viscous flow below the deck adjacent to the wall is governed by the Linearized Unsteady Boundary Layer Equation, revealing that the energy transition from the wave-length of the freestream disturbance to that of the instability waves is mainly caused by the short-scale nonparallel flow effects. Kerschen et al. [6] examined receptivity induced by two-dimensional suction trips and interaction of vertical freestream disturbances with wall inhomogenisities [8], Choudhari et al. [7] extended their work to three-dimensional inhomogeneous wall. Crouch [9] further developed localized receptivity analyses by considering parallel shear flow with only small disturbances. Duck et al. [10] by using a triple-deck formulation analyzed the receptivity of interaction between a vortical disturbance and a roughness. Based on the same Orr-Sommerfield equations, Choudhari et al. [11] studied the same kind of interactions studied by Duek et al. [10]. Their calculation showed that the lower-frequency components of the gust could be a more effective T-S wave generator.

Many experiments have been conduced to verify the theoretical results of receptivity of incompressible boundary layers to two-dimensional roughness. Welzien et al. [12, 13] did experiments measure on the acoustic receptivity to porous suction slots. Saric et al. [14] studied the receptivity of two-dimensional roughness to acoustic waves with minimal leading-edge effects. Two-dimensional roughness trips with 40-um thick and 25-mm wide were used. The width of strip is identical to the half wavelength of the T-S wave ($\lambda_{TS} = 50mm$) and $F = 50$. They correlated the effect of thickness of the roughness element with a roughness Reynolds number R_k . In Saric's paper, R_k is based on the local velocity and the roughness height k , where $R_k = U(k)k / v$ .With the variation of roughness height k it was found that the T-S amplitude increase linearly with the roughness in the range of $40-120\mu m$. This linear behavior was also predicted by Crouch [15] and Nayfed et al. [16]. The departure from linear behavior occurs in the range of $k = 180-255\mu m$, which was validated by Bodonyi et al. [17] by a nonlinear triple-deck analysis. Kerschen et al. [6] analyzed localized receptivity due to porous suction trips and showed that these two kinds of receptivity mechanism are fundamentally the same. Kosorygin et al. [18] reported experiments results about where the position of roughness was changed with respect to the leading edge. His research work showed that there exists a particular x position where the destructive interface is a maximum and the T-S wave amplitude is below the leading-edge(no roughness) value. Kosorygin [19] then extended this work by taking the adverse and favorable pressure gradient into account.

There have been limited reported numerical simulation studies of boundary-layer receptivity to surface roughness. For problems having complex computational geometry, as might occur in the transition problems induced by isolated/distributed roughness, the use of body fitted curvilinear gird could prove to be very difficult due to natural complexities in grid generation. Consequently, one approach for overcoming this difficulty is to use a Cartesian cut cell method, which is easy in generating and implementing numerical schemes. Cut cell methods can take full advantage of fast computer architectures like vector or parallel computers and could serve as a very flexible method for simulating flow around complex geometries. It was first used for solving the equations of transonic potential flow by Purvis and Burkhalter [28]. Then it was further developed to calculate steady compressible flows by Clarke et al. [29]. Among those applications, a problem referring to restriction on time step would arise when we are trying to implement high-order numerical scheme in relatively small-size irregular cell. This constriction which is termed as "small cell problem", would significantly delay the temporal advancement, as well as increasing the computational cost. Thus the major issues is on how to design a method that could not only relax the time step, but also maintain the overall accuracy, stability, and conservation of numerical results inside the irregular cells.

Many innovative methods were developed to resolve the small cell problem. Berger and Leveque [30] used rotating box metho. Colella et al. [31-33] used flux-redistribution procedures, and Quirk [34], Shyy [35] used cell merging method to get numerical stability. However, all the cut cell methods with different treatments to the boundary were of first or second order, which were not sufficient in numerically simulating laminar-turbulent boundary transitions. Shyy et al. [37] extended his previous second-order method to fourth order with merging cell approach. But the reconstruction flux procedure is relatively expensive thus slowing down the computational efficiency. Colella et al. [38] developed a fourth-order accurate finite volume method combined with a local mesh refinement for discretizing Poisson's equation in a rectangular domain. However, this kind of method could be tedious in implementing for irregular domain. Fedkiw et al. [39] also presented a fourth-order finite difference method for solving the Laplace equation on an irregular domain by using the ghost fluid method. The key point of his method is to extrapolate the existing flow variables into the artificial nodes outside the boundary where the same high-order uniform finite difference scheme could be executed.

In this paper, we present a high-order cut-cell method. A non-uniform finite difference technique is developed to calculate the flux vector in the irregular grid cells. The new method is applied to Mach 5.92 flow over two-dimensional flat plate. The bow shock generated from the leading edge of the flat plate will be treated as a boundary condition and discretized based on Zhong's [41] fifth-order finite difference flux split method and shock fitting method. We first obtain the steady state solution with a surface roughness placed on the flat plate 0.186m downstream with height to be half of boundary-layer thickness. For unsteady solution, the flat plate with a blow-suction composed of 15 different frequencies mounted at 0.030m downstream from the leading edge is simulated.

II. Governing Equations

The governing equations for the numerical simulation of hypersonic boundary layer transition are the three-dimensional Navier–Stokes equations. We assume that we are dealing with Newtonian fluids with perfect gas assumption and adiabatic wall condition. The governing equations can be written in the following conservation-law form in the Cartesian coordinates.

$$\frac{\partial U}{\partial t} + \frac{\partial F_j}{\partial x_j} + \frac{\partial F_{vj}}{\partial x_j} = 0 \tag{1}$$

where U , F_j and F_{vj} are the vectors of flow variables, convective flux, and viscous flux in the j th spatial direction respectively, i.e.,

$$U = \left\{ \rho, \rho u_1, \rho u_2, \rho u_3, e \right\} \tag{2}$$

$$F_j = \begin{Bmatrix} \rho u_j \\ \rho u_{j1} u_j + p\delta_{1j} \\ \rho u_{j2} u_j + p\delta_{1j} \\ \rho u_{j3} u_j + p\delta_{1j} \\ (e+p)u_j \end{Bmatrix} \tag{3}$$

$$F_{vj} = \begin{Bmatrix} 0 \\ \tau_{1j} \\ \tau_{2j} \\ \tau_{3j} \\ \tau_{jk} u_k - q_j \end{Bmatrix} \tag{4}$$

In this paper, only perfect-gas hypersonic flow is considered, i.e.,

$$p = \rho RT \tag{5}$$

$$e = \rho(C_V T + \frac{1}{2} u_k u_k) \tag{6}$$

$$\tau_{ij} = \mu(\frac{\partial u_i}{\partial x_j} + \frac{\partial u_j}{\partial x_i}) + \delta_{ij} \lambda \frac{\partial u_k}{\partial x_k} \tag{7}$$

$$q_j = -k \frac{\partial T}{\partial x_j} \tag{8}$$

where R is the gas constant. The specific heats C_V are assumed to be constants with a given ratio of specific heats γ . The viscosity coefficient μ can be calculated by Sutherland's law in the form:

$$\mu = \mu_r (\frac{T}{T_0})^{3/2} \frac{T_r + T_s}{T + T_s} \tag{9}$$

and , λ is assumed to be $-2/3\mu$. The heat conductivity coefficient γ can be computed through a constant Prantl number Pr.

III. Numerical Methods

A. Discretization in Space – High-Order Finite Difference and Shock-Fitting Method

To satisfy the accuracy requirement for capturing small disturbances inside the boundary layer for receptivity and transition simulation, a three-dimensional fifth-order shock-fitting method developed by Zhong is used to compute the flow field bounded by the bow shock and wall surface. In the discretization of the Navier-Stokes equations, spatial derivatives in the streamwise (s) and wall-normal (y_n) directions are modeled by a fifth-order finite difference scheme. The flow variables behind the shock are determined by the Rankine-Hugoniot relations across the shock and a characteristic compatibility equation from behind the shock. The details of the shock fitting formulas and numerical methods can be found in [41].

The proposed numerical scheme will base on this finite difference method, thus the governing equation (1) is transformed into the computational domain (ξ, η, ζ, τ) as

$$\frac{1}{J}\frac{\partial U}{\partial \tau} + \frac{\partial E'}{\partial \xi} + \frac{\partial F'}{\partial \eta} + \frac{\partial G'}{\partial \zeta} + \frac{\partial E_v'}{\partial \xi} + \frac{\partial F_v'}{\partial \eta} + \frac{\partial G_v'}{\partial \zeta} = 0 \tag{10}$$

where

$$E' = \frac{F_1\xi_x + F_2\xi_y + F_3\xi_z}{J} \tag{11}$$

$$F' = \frac{F_1\eta_x + F_2\eta_y + F_3\eta_z}{J} \tag{12}$$

$$G' = \frac{F_1\zeta_x + F_2\zeta_y + F_3\zeta_z}{J} \tag{13}$$

$$E_v' = \frac{F_{v1}\xi_x + F_{v2}\xi_y + F_{v3}\xi_z}{J} \tag{14}$$

$$F_v' = \frac{F_{v1}\eta_x + F_{v2}\eta_y + F_{v3}\eta_z}{J} \tag{15}$$

$$G_v' = \frac{F_{v1}\zeta_x + F_{v2}\zeta_y + F_{v3}\zeta_z}{J} \tag{16}$$

As shown in Fig.1, standard finite difference scheme will base on Equation (10)-(16).

B. Treatment of Fluid-Solid Boundary – Cut Cell Method

In traditional Cartesian cut cell method [30-35], rectangular Cartesian cells are generated to fulfill the irregular computational domain directly. In order to improve the computational efficiency, in our numerical process the physical domain without roughness is transformed and projected onto a regular domain at first as shown in Fig. 1. This transformation procedure can eliminate the unnecessary irregular cells formed through intersections of girds lines and curvilinear solid wall boundary.

After the coordinate transformation, the two-dimensional computational domain is cut uniformly by the vertical and horizontal girds line and divided into both small regular and irregular Cartesian cells. Four different kinds of girds located in the vertex of those Cartesian cells are defined and different numerical algorithm is implemented. The four different kinds of girds are regular point, irregular point, boundary point, and dropped point as shown in

Fig. 2. The intersections of roughness interface and girds lines are defined as boundary points. The other points come from intersections of girds lines themselves are termed as regular points, irregular points and dropped points respectively. The criteria for distinguishing those are depending on their minimum distances to the solid wall. If the grids points adjacent to a boundary point with a distance smaller than a pre-specified critical ratio (e.g. $\Delta h/10$) in x or y direction, they are defined as dropped points in this x or y direction and was took off from the gird stencil in later stage. For those points whose finite difference stencil may include boundary points, they are defined as irregular points. Then the left points are defined as regular points since they are relatively far away from boundary points, where a standard uniform finite difference method can be used.

The flux terms in regular points are computed by the traditional high-order upwind finite difference scheme [41], which might take up to a seven point stencil. To calculate the flux in irregular points, a non-uniform finite difference method is used, whose stencil is consisted of regular, irregular and boundary points. Noting the points marked with red dot in Fig. 2 are dropped, they should not be included into this non-uniform stencil. As a result, the small segment in a non-uniform difference stencil between the dropped point and irregular point are enforced to merge into a large segment which connects the nearby boundary point and irregular point directly. This kind of grids definition and segment merging approach ensure that distance between two adjacent grids in the seven points stencil to be large enough for maintaining the overall stability within acceptable time step range. This cut cell method is conservative, easy to implement, high efficiency, and suitable for computing hypersonic boundary receptivity and transition problems with strong shocks.

The numerical scheme in irregular points involve in non-uniformly finite difference stencil. Typically, to obtain N^{th} order global accuracy, a $N-1$ grids stencil should be adapted as shown in Fig. 4 (Labeled from 2 to $N/2+1$). To maintain the consistence to the original uniform finite difference method, a non-uniform flux-split method is developed to separate the flux variable at irregular points into positive and negative part. Both of the upwind and backwind non-uniform difference schemes will be applied into the two parts separately. The non-uniform finite difference formulation for different irregular points is derived though taking first-order derivatives to Lagrange interpolation polynomial as shown in (17) for corresponding irregular points. Similarly, the second-order numerical derivative is obtained by taking another first-order derivative toward formulation in (17).

$$\begin{cases} \left[\frac{\partial u}{\partial x}\right]_{x=x_{n/2+1}} = \frac{1}{\Delta\xi}\sum_{k=-n/2-1}^{n/2+1} a_{n+k}u_{n+k} - \frac{\alpha}{(n+1)!}\Delta\xi^{n}\left(\frac{\partial u^{n}}{\partial^{n+1}u}\right) + \text{.....} \\ \left[\frac{\partial u}{\partial x}\right]_{x=x_{n/2}} = \frac{1}{\Delta\xi}\sum_{k=-n/2}^{n/2} a_{n-1+k}u_{n-1+k} - \frac{\beta}{(n+1)!}\Delta\xi^{n-1}\left(\frac{\partial u^{n-1}}{\partial^{n}u}\right) + \text{.....} \\ \text{.....} \\ \left[\frac{\partial u}{\partial x}\right]_{x=x_{1}} = \frac{1}{\Delta\xi}\sum_{k=0}^{n-2} a_{1+k}u_{1+k} - \frac{\beta}{(n+1)!}\Delta\xi^{n-1}\left(\frac{\partial u^{n-1}}{\partial^{n}u}\right) + \text{.....} \end{cases} \quad (17)$$

In equation (17), a_k represent coefficients derived through the N–1th order Lagrange interpolation polynomials after taking one-order derivatives with respect to x. Since all the coefficients are depending on the metrics of moving girds caused by shock-fitting method, at each time step the value of those points should be recalculated. A similar scheme parameter α in terms as forward/backward coefficient is also defined as it is in uniform scheme for the the non-uniform finite difference scheme.

High-order finite difference method requires numerical boundary conditions of comparable order to maintain global accuracy. To maintain N^{th} order accuracy, at least N–1th order boundary closure is needed. Specifically, to maintain the stability and global computational errors in fifth-order, it is desirable to have at least fourth-order accuracy in boundary. And in terms of solving viscous layer effect, more girds near the boundary in the domain should be clustered in the finite difference stencil. The unsteady shock interface in the upper bound is treated by shock-fitting method. The boundary conditions can be determined by the Rankine-Hugonion condition. Since the freestream condition is hypersonic, the characteristic lines in flow field are all pointing towards same directions without any waves propagating back into interior. Thus a high-order extrapolation up to fourth-order is used for obtaining outlet boundary conditions for all flow variables without introducing any numerical instability.

Non-slip adiabatic wall boundary condition is applied to the solid interface with surface roughness. Since there is a singularity while using shock-fitting method in the computational region containing leading edge, our numerical

simulation with non-uniform scheme will be carried on in the downstream far from the leading edge. It turns out that the boundary layer in our computational zone is fully developed, and two additional boundary conditions are needed as follows,

$$\frac{\partial P}{\partial n} = 0, \quad \frac{\partial T}{\partial n} = 0 \tag{18}$$

where n is the coordinate along the wall-normal direction. In our later receptivity simulation, we set the boundary condition for temperature perturbation to be zero, since the frequency of disturbance is so high that the solid wall can not respond in such high frequency.

Equations (10) are discretized by N–1^{th} order one-sided finite difference method along the local normal vector near surface. The stencil is entirely located in fluid part with first point being the boundary point.

A close attention should be paid to boundary points where the finite difference stencil is not uniform. Let l denotes the distance between two adjacent points, e.g. l_1 connects point 1 and 2, l_2 connects point 2 and 3 as shown in Fig. 3. After applying one-sided high-order difference scheme toward boundary points, linear equations can be derived as (19) and (20). This type of high-order extrapolation is very sensitive to the critical ratio and serves as a crucial factor for overall numerical simulations stabilities. Further extensive numerical tests on this factor are necessary to investigate their influences.

$$P(l) = \sum_{i=2,n} \frac{\prod_{j=2,n-1} (l - l_j)}{\prod_{j=2,n-1} (l_i - l_j)} P_i \qquad l = l_1 \tag{19}$$

$$T(l) = \sum_{i=2,n} \frac{\prod_{j=2,n-1} (l - l_j)}{\prod_{j=2,n-1} (l_i - l_j)} T_i \qquad l = l_1 \tag{20}$$

Finite difference method for regular/irregular point may involve in dropped points rather than the pre-specified dropped direction. To achieve global conservation of the governing partial difference equation, we should recover the flux in dropped points at each time step. The key point of this recover process is to use a N^{th} order non-uniform linear interpolation to obtain the numerical value from flow variables along the local normal vector near the dropped points.

IV. Results and Discussions

A. Steady Base Flow without Roughness

A test case for flow over a two-dimensional flat plate with Mach number 5.92 without roughness is conducted. The numerical results are used to compare with the case without roughness element applied in the flow field.

The steady mean flow solutions are calculated by using a fifth-order shock fitting method. But in the leading edge of the flat plate, there is a singularity when high-order shock fitting method is implemented. Thus a second-order TVD shock-capturing method is initialized to calculate the flow field in the tip of flat plate. The computational domain for TVD starts from a very short distance downstream of the leading edge which is divided to 100×200 grids. The ambient flow conditions are:

- $M_\infty = 5.92, T_\infty = 350.0K, P_\infty = 3903.5Pa$
- $P_r = 0.72, R^*_{e\infty} = \rho_\infty * u_\infty / \mu_\infty = 1.32 \times 10^6 / m$
- $-0.0006 < x < 0.0030m$

(21)

The flat plate is assumed to be adiabatic. The spatial discretization of TVD scheme is applied toward equation (10) and leads to semi-discrete system of ordinary differential equations, which are solved by using second-order Runge-Kutta method.

To validate the numerical simulation results, we use parameters after the shock to non-dimensionalize the flow field and compare the numerical and analytical solutions at $x = 0.001m$ in Fig. 5. A good agreement between these two results is achieved. The minor difference outside the boundary layer is caused by the shock generated by the leading edge. The two-dimensional flow field then could serve as inlet condition for the fifth-order shock fitting code.

The computational domain for the fifth-order shock-fitting methods starts at $x = 0.003m$ and ends at $x = 1.68784m$. In actual simulations, the computational domain is divided into 30 zones, with total of 5936 grid points in the stream wise direction, and 121 points in the vertical direction. An exponential stretching function is used for coordinate transformation in the vertical direction in order to cluster more girds inside the boundary layer. As mentioned above, the second zone uses the results of the first zone of second-order TVD scheme as the inlet condition. The later zone used the interpolation of former zone's data as the inlet condition.

In zone 8, computational domain starts at $x = 0.159m$ and ends at $x=0.195m$. Pressure and velocity contours for zone 8 have been plotted in Fig. 6. The numerical solution is bounded by oblique shock and laminar boundary layer near the plate. Fig. 7 shows the horizontal velocity profile and temperature profiles in the vertical direction at the location of $x = 0.1676m$. The current numerical solutions are compared with the self-similar boundary layer solution. The velocity and temperature are normalized by corresponding freestream value, while y is nondimensionalized by $\sqrt{x\mu/\rho U}$. These figures show that the results of the current numerical simulation agree very well with theoretical solution. Thus second-order TVD scheme is accurate enough to be the supporting inlet condition of fifth-order shock-fitting method.

B. Steady Flow with Roughness

A pinhead like roughness shape is used on the surface of plate at downstream $x = 0.186m$. The shape of the roughness is following Whiteheard's experiments [43]. The surface roughness is modeled as a two-dimensional bump, governed by the elliptic equation:

$$(x - x_c)^2 / a + by^2 = h^2 \tag{22}$$

The computation are performed under parameter configuration $a = 4,\ b = 1$ and $h/\delta = 1/2$ where δ corresponds to the boundary layer thickness at $x_c = 0.186m$ as shown in Fig. 8a. Cartesian meshes are generated to discretize the entire computational domain as shown in Fig. 8b. A girds stretching function is also employed to concentrate more girds in boundary layer to gain better resolution in viscous layer.

Fig. 9 shows the pressure and Mach number contours in zone 8 where the roughness located in. A bow shock appears in front of bump and extends along the streamwise direction to outside the domain. Along the surface of roughness, the pressure reach the minimum at the tail since the coming fluids is compressed by the roughness at the beginning, and then is expanding along the downstream. Fig. 10 shows the pressure and Mach number contour from zone 8 to zone 10. Instead of increasing, the shock strength keeps decreasing all the way to the downstream. The initially disturbance is damped away in zone 9. The laminar-turbulence transition did not present in our numerical simulation, due to the low order accuracy, finite Reynolds Number, approximated boundary conditions et al.

Fig. 11-13 show the horizontal velocity and density profiles along a wall-normal vector at location $x = 0.188m$, $x = 0.200m$ and $x = 0.240m$ for flow without and with roughness height $h/\delta = 1/2$ respectively. Steady solutions are obtained for all cases and there is not any vortex shedding is observed. The mean flow is distorted immediately after the roughness and a main steady perturbation begins to form and evolutes downstream. The amplitude of main steady perturbation is significant compared with the boundary layer initially but begin to diminish as it goes downwards. At $x = 0.240m$ the magnitude of this modification to base blow is reduced by half but the sine wave like main shape is preserved. It is suggested that so far no transient growth is observed, which is consistent with Tumin's conclusion for two-dimensional roughness. Along the downstream direction, the main roughness perturbation is moving upward constantly with some small secondary stability waves developed inside of it. It is suggested that the steady disturbance is generated from mechanism that distorting the mean flow by

the shock wave which induced by hypersonic flow over curvilinear roughness surface. Thus the energy of the shock wave would be dissipated by the viscous effect slowly and the base flow modification will eventually disappear.

Fig. 14 shows the evolutions of streamwise velocity and pressure perturbation in the downstream at different locations. Compared with mean flow, there is minor difference in the streamwise velocity but a clearly velocity deficient which induced by roughness can be observed. From the upstream to the downstream of the roughness the boundary layer become thicker than the mean flow case thus it turns out that the receptivity process in the boundary layer with roughness effect can be different. An overall schematic of pressure modification evolution could be found in Fig. 14b. Initially the boundary inhomogenisities develops a sine curve like perturbation, and as it go downstream, the perturbation moves upwards as well as stretching in wall-normal direction. Eventually at $x = 0.240m$ many tiny instability waves excited by flow impinge roughness initially are amplified and disturb the main perturbation in terms of wave interactions. During the wave developing process, the amplitude of main perturbation wave is keeping decreasing which is partially caused by the lift up theory and viscous dissipations. Fig. 15 exhibits the pressure and Mach number profile along the streamwise direction at fixed $y = 0.010m$. From $x = 0.200m$ to $x = 0.240m$ the pressure and Mach number of mean flow is remaining to be nearly unchanged. Compared with the mean flow, pressure with roughness effect is amplified firstly by the shock wave and then diminished through the expansion wave generated from interaction of hypersonic flow and curvilinear roughness surface.

Current computations suggest that with the roughness effect the flat-plate boundary layer can become thicker in the downstream compared mean flow case thus a different Mack mode instability mechanism can be introduced. But the perturbations from roughness effect with $h/\delta = 1/2$ are keeping decaying in present simulation, which say that the disturbance is not strong enough to lead to bypass transition and transition to turbulence directly.

C. Unsteady Flow with Roughness

A blow-suction slot is imposed as periodic-in-time boundary conditions for the perturbation of the mass flux on the wall. The blow-suction is located at $x = 0.030m$ and spread over several girds spaces. The perturbation is controlled by the function:

$$\rho v = q_0 g(l) \sum_{n=1}^{15} \sin(w_n t) \tag{23}$$

where q_0 is an amplitude parameter and w_n is circular frequency of this multi-frequency perturbation. $g(l)$ is non-dimensional x-direction profile function defined as

$$g(l) = \begin{cases} 20.24l^5 - 35.4375l^4 + 15.1875l^3 & (l < 1) \\ -20.24(2-l)^5 + 35.4375(2-l)^4 - 15.1875(2-l)^3 & (l \geq 1) \end{cases} \tag{24}$$

The variable is the non-dimensional parameter associated with current coordinate of this blow-suction,

$$l(x) = \frac{2(x - x_i)}{(x_e - x_i)} \tag{25}$$

A fifth order shocking fitting method combined with high order upwind finite difference scheme is used for computing the unsteady Mach number 5.92 flow over flat plate with blow-suction located near the leading edge without surface roughness. At the beginning of simulation, a basic frequency $f_1 = 50kHz$ is specified and the other 14 different frequencies are integer times the basic frequency as $n = 2, 3, 4....$ *or* $f = 100, 150, 200...$ *kHz* . This case is similar to the cases studied by Wang et al. [44]. More details can be found in that paper.

Fig. 16 shows the pressure disturbance for the overall unsteady flow from zone 3 to zone 10. Fig. 17 shows the contours for pressure and horizontal velocity disturbance in zone 8. The amplitude of disturbance is very strong initially due to the periodic injection of mass flux and then it starts to decay fast outside the boundary layer. This damping behavior of large perturbations is very similar to the roughness effect which is considered to be caused by viscous dissipations. Due to the external unsteady disturbance, there are some instability waves possess typical T-S wave like characteristic excited inside the boundary layer via receptivity process. The T-S waves, after experiencing transitional first mode instability in the upstream, begin to grow fast in zone 8 which is shown in Fig. 17. It turns out a second mode instability is excited for the T-S waves inside the downstream of flat-plate boundary layer.

Fig. 18 shows the contours for pressure and horizontal velocity disturbance in zone 8 for flow over flat plate with surface roughness. There is no second mode instability behavior for T-S waves inside the boundary layer observed. The magnitude of T-S wave diminished at the beginning of zone 8 and finally damped out. Fig. 19 show the maximum magnitude of horizontal velocity disturbance along the streamwise direction with respect to different frequency, e.g. $n = 2, 3, 4, 5$. A Fast Fourier Transformation (FFT) technique is employed to separate all the disturbances with different frequency. For the simulation of case without roughness, two behaviors of evolution of T-S waves are observed. The first one is that the amplitude of T-S waves of some frequencies oscillates in the x direction but its variation remains within a small range, which suggests a first mode like evolution. The other kind of behavior is that the amplitude keeps amplifying and increasing monotonely. As shown in Fig. 19b, the growth rate of streamwise velocity disturbance reach the maximum at frequency $f = 150kHz$. It implies that a second Mack instability mode is excited at this specified location of flat plate and freestream disturbance frequency, which is consistent with our theoretical intuitions. But as Fig. 19 shown, very different from traditional normal modal linear instability analysis and case without roughness, for case with surface roughness the amplitude of T-S waves with various frequencies begin to decay exponentially from the inlet of zone 8 and finally are damped out fast. Around the surface roughness Fig. 19a exhibits a different amplitude evolution behavior at frequency $f = 100kHz$ from the other three. Rather than decaying, the wave amplitude is amplified moderately around the roughness thus we might deduce that surface roughness plays a destabilizing effect in boundary-layer linear stability theory.

Considering the differences between the case with and without roughness, it should be pointed out that the results at this stage are still preliminary. Further studies are needed to explain the significant decay of the instability wave due to roughness in this case.

V. Conclusions and Future Plans

A test case of Mach number 5.92 flow over flat plate with surface roughness has been conducted by using the high-order cut-cell method. The receptivity process induced by the interaction of blow-suction and flat plate with roughness is also numerically investigated.

Due to the existence of surface roughness, the hypersonic flow is compressed and a weak oblique shock is formed in front the roughness and then an expansion waves is followed. There is a significant change of flow profiles inside the boundary layer in the downstream of surface roughness. But the modification to basic flow keeps decaying outside the boundary layer. The receptivity to surface roughness induced by blow-suction roughness is also investigated but the computational results are still very preliminary. Further extensive numerical experiments for current configurations are needed to obtain more substantial results.

Acknowledgments

This work was sponsored by the Air Force Office of Scientific Research, USAF, under AFOSR Grant #FA9550-07-1-0414, monitored by Dr. John Schmisseur. The views and conclusions contained herein are those of the author and should not be interpreted as necessarily representing the official policies or endorsements either expressed or implied, of the Air Force Office of Scientific Research or the U.S. Government.

References

1. E. Piot, G. Casalis and M. Terracol , *Direct numerical solution of the crossflow instabilities Induce by a Periodic Roughness Array on a swept cylinder: receptivity and stability investigations*, 37th AIAA Fluid Dynamics Conference and Exhibit, Miami, FL, June 25-28, 2007 No. 1, 1999, pp. 134-150
2. S. Berry and T. Horvath, *Discrete roughness transition for hypersonic flight vehicles* , 45th AIAA Aerospace Sciences Meeting and Exhibit, Reno, Nevada, Jan. 8-11, 2007
3. Malik, M.R., Spall, R. E., and Chang, C. L., *Effect of nose bluntness on boundary layer stability and rransition.* 1990. AIAA Paper 90-0112.
4. William S.Saric, Helen L. Reed, and Edward J.Kerschen, *Boundary-layer receptivity to freestream disturbances*, Annu. Rev. Fluid Mech, 2002.34:291-319

5. Goldstein ME. 1985. *Scattering of acoustic waves into Tollmien-Schlichting waves by small streamwise variations in surface geometry*. J. Fluid Mech. 154:509–29
6. Kerschen EJ, Choudhari M, Heinrich RA. 1990. *Generation of boundary instability waves by acoustic and vortical freestream disturbances.* See Arnal & Michel 1990, pp. 477–88
7. Ellingsen, T. and Palm, E., *Stability of linear flow*, Phys. Fluids, Vol. 18, No. 487, 1975.
8. Landahl, M. T., *A Note on an algebraic instability of inviscid parallel Shear flows*, J. Fluid Mech.,Vol.8, 1980, pp. 243-251.
9. Trefethen, L., Trefethen, A., Reddy, S., and Driscoll, T., *Hydrodynamic stability without eigenvalues*, science, Vol. 261, 1993.
10. Henningson, D., *Bypass transition and linear growth mechanisms*, Advances in TurbulencV, edited by R. Benzi, Kluwer, 1995.
11. Reshotko, E., *Transient growth—A factor in bypass transition*, Phys. Fluids, Vol. 13, No. 5, 2001,pp. 1067-1075.
12. Wlezien RW. 1989. *Measurement of boundary layer receptivity at suction surfaces.* AIAA Pap. 89–100
13. Wlezien RW, Parekh DE, Island TC. 1990. *Measurement of acoustic receptivity at leading edges and porous strips.* Appl. Mech. Rev. 43 (Pt. 2): S167–74
14. Saric WS, Hoos JA, Radeztsky RH Jr. 1991. *Boundary-layer receptivity of sound with roughness.* See Reda et al. 1991, pp. 69–76
15. Crouch JD. *Initiation of boundary-layer disturbances by nonlinear mode interactions.* See Reda et al. 1991, pp. 63–68, 1991
16. Nayfeh AH, Ashour ON. 1994. *Acoustic receptivity of a boundary layer to Tollmien- Schlichtingwaves resulting from a finiteheight hump at finite Reynolds numbers.* Phys. Fluids *A* 6:3705–16
17. Bodonyi RJ. 1990. *Nonlinear triple-deck studies in boundary-layer receptivity*. Appl. Mech. Rev. 43 (Pt. 2):S158–66
18. Kosorygin VS, Radeztsky RH Jr, Saric WS. *Laminar boundary layer sound receptivity and control*.See Kobayashi, pp. 517–24, 1995.
19. Kosorygin VS. *Experiments on receptivity, stability, and transition of twodimensional laminarboundary layers with streamwise pressure gradients*, 2000, pp. 97–102
20. White, E. B., and Ergin, F. G., *Receptivity and rransient growth of Roughness-Induced disturbances*, AIAA Paper 2003-4243, 2003.
21. White, E. B., Rice, J. M., and Ergin, F. G., *Receptivity of stationary transient disturbances to Surface roughness*, Physics of Fluids, Vol. 17, No. 6, 2005, 064109.
22. White, W.B., *Receptivity of transient growth to surface roughness*, AIAA JOURNAL Vol. 44, No.11, November 2006
23. Kendall, J., *Laminar boundary layer Velocity Distortion by Surface Roughness: Effect upon Stability*, AIAA Paper 81-0195, 1981.
24. M. Choudhari, *Roughness-Induced transient growth*, 35th AIAA Fluid Dynamics Conference and Exhibit, Toronto, Ontario, June 6-9, 2005
25. P. Fischer, *Numerical simulation of Roughness-Induced transient growth in a laminar boundary layer* , 34th AIAA Fluid Dynamics Conference and Exhibit, Portland, Oregon, June 28-1, 2004 108
26. E. Piot, G. Casalis and M. Terracol, *Direct Numerical Solution of the Crossflow Instabilities Induced by a Periodic Roughness Array on a swept cylinder: receptivity and stability investigations*, 37th AIAA Fluid Dynamics Conference and Exhibit, Miami, FL, June 25-28, 2007
27. Donald P. Rizzetta; Miguel R. Visbal, *Direct numerical simulations of flow past an array of distributed roughness elements*, AIAA Journal 2007 0001-1452 vol.45 no.8 (1967-1976)
28. J.W.Purvis and J.E.Burkhalter, *Prediction of critical Mach number for store configurations* AIAA J. 17, 1979
29. D.K.Clarke, M.D.Salas, *Euler calculations for multielement airfoils using Cartesian grids* AIAA J.24, 1986
30. M.J.Berger and R.J.Leveque, *Stable boundary condition for Cartesian grid calculations*, Computing System,1990
31. Hans Johansen, Phillip Colella, *A Cartesian grid embedded boundary method for poisson's equation*, J. Comput. Phys, 1998
32. Pember, Bell, Colella et al., *An adaptive Cartesian grid method for unsteady compressible flow irregular Regions*, J. Comput. Phys, 2006

33. Colella et al., *A node-centered local refinement algorithm for poisson's equation in complex geometries*, J. Comput. Phys,2004
34. James J. Quirk, *An alternative to unstructured girds for computing gas dynamic flows around arbitrarily complex bodies*, Comp. Fluids, 1994
35. T. Ye, R. Mittal, H. S. Udaykumar and W. Shyy, *An accurate Cartesian grid method for viscous incompressible flows with complex immersed boundaries*, J. of Compu. Physics, *Volum. 156, Issue 2, 10 December 1999, Pages 209-240*
36. Hans Forrer and Rolf Jeltschy , *A higher-order boundary treatment for Cartesian-grid methods* , J. Comput. Phys, 1997
37. M,Popescu et al., *A finite volume-based high order Cartesian cut-cell method for computational aeroacoustics*, AIAA Paper, 2005
38. Michael Barad, Phillip Colella, *A fourth-order accurate local refinement method for poisson's equation*, J. Comput. Phys, 2005
39. Gibou, Fedkiw, *A fourth order accurate discretization for laplace and heat equations on arbitrary domain*, J. Comput. Phys, 2004
40. DD.Zeeuw and KG.Powell, *An adaptively refined Cartesian mesh solver for the Euler equations*, J. Comput. Phys, 1993
41. X.Zhong, *High-order finite-difference schemes for numerical simulation of hypersonic boundary- layer transtion*, J. Comput. Phys 144 , 1998
42. J. H. Williamson, *Low-storage Runge–Kutta schemes*, *J. Comput. Phys.* 35, 48 (1980).
43. A.H. Whitehead, Jr. *Flowfield and drag characteristics of several boundary-layer tripping elements in hypersonic flow*. Techinical Note TND-5454, NASA October 1969
44. A. Tumin, X. Wang, and X. Zhong, *Direct numerical simulation and the theory of receptivity in a hypersonic boundary layer*, Physics of Fluids, 19, 014101, 2007

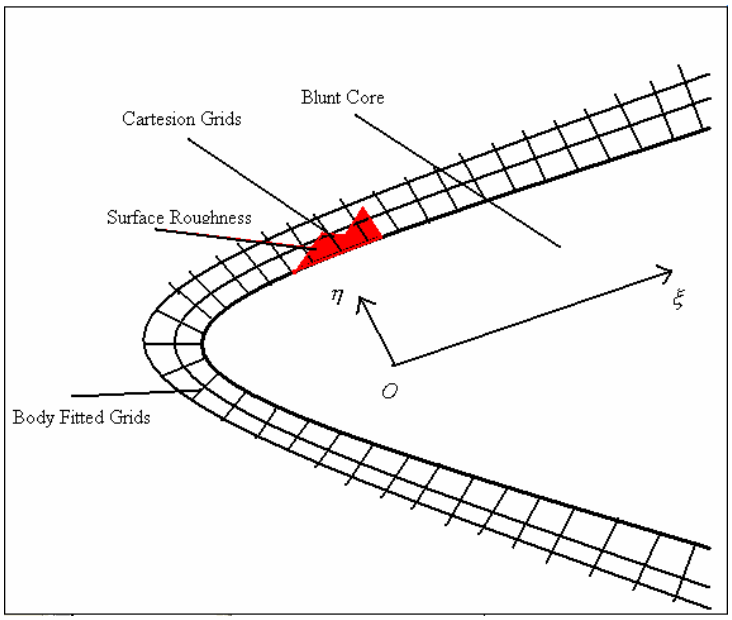

Figure 1. *Body-fitted grids for flow over a blunt core with finite surface roughness.*

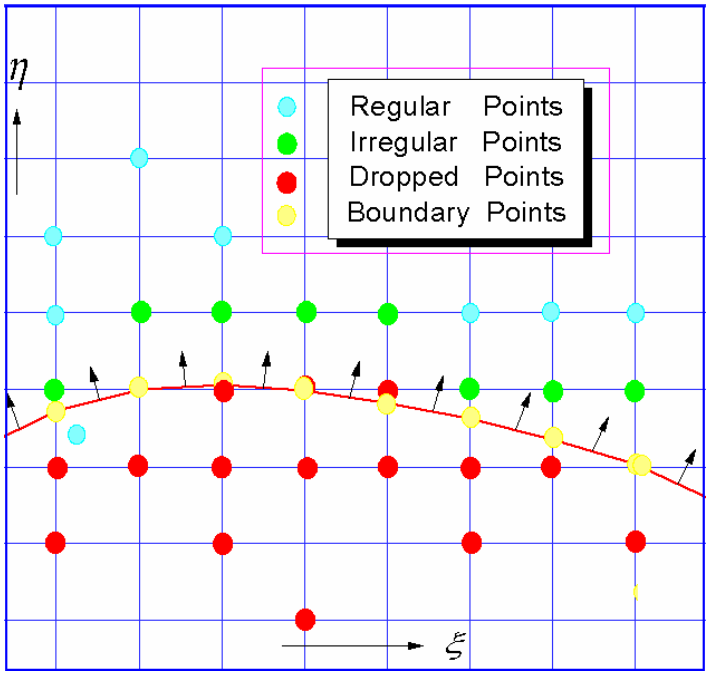

Figure 2. *Definition of girds for high-order cut cell method. Four kinds of girds are defined. The intersections of roughness and curvilinear girds form the boundary points and marked with yellow dot. When the grids are too close to a boundary point in one direction, they are defined as dropped points and marked with red dots. The irregular points are involving in non-uniform finite difference stencil and marked with green dots. The rest points are regular points and marked with blue dots.*

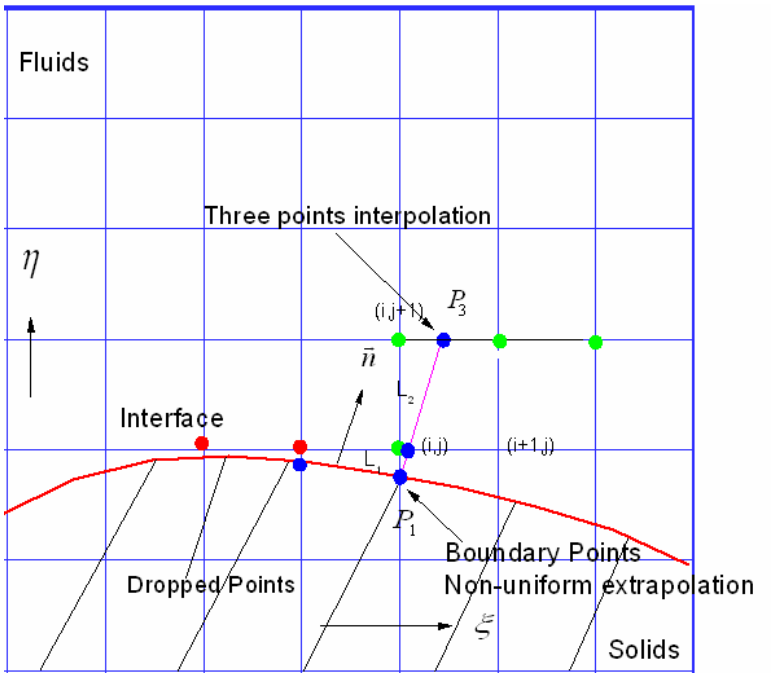

Figure 3. *Schematic of computational methodology for boundary points. Blue dots represent one side* N^{th} *order finite difference stencil for boundary points. Green dots represent N th order interpolation stencil for blue dots.*

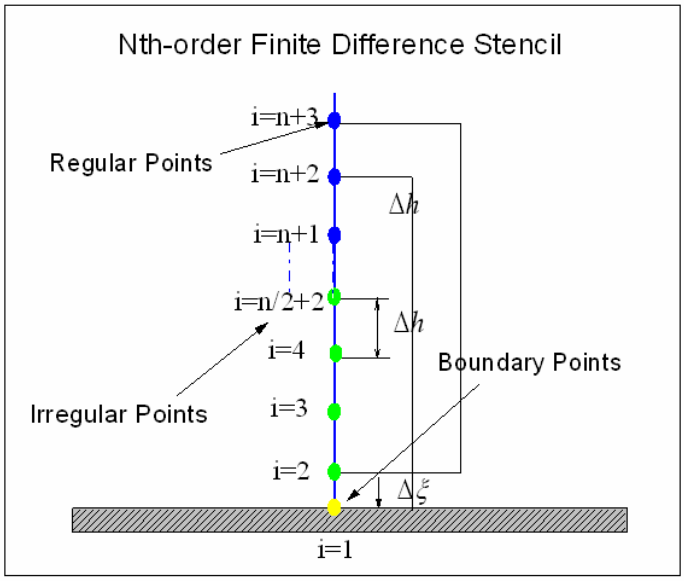

Figure 4. N^{th} *order non-uniform finite difference stencil for irregular points.*

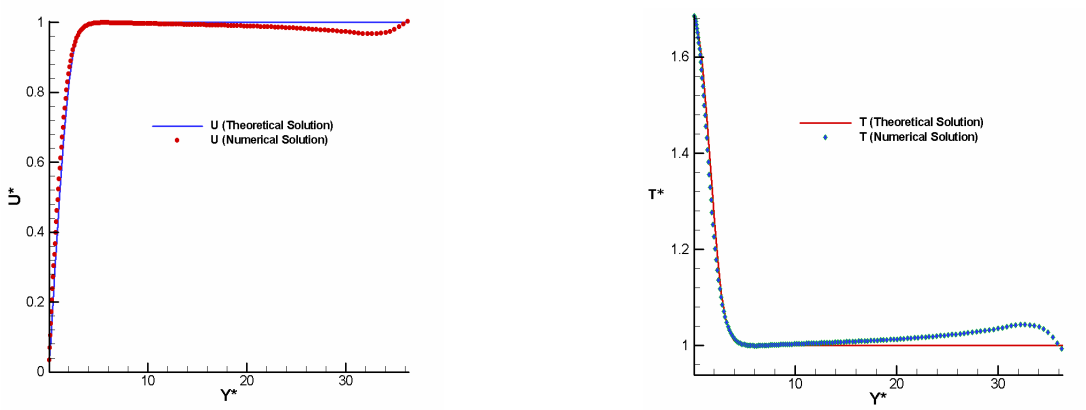

Figure 5. *Along a wall-normal grid line which is originated from a point located at* $x = 0.001m$ *on the plate surface. (a), temperature (b),velocity in y direction profile.*

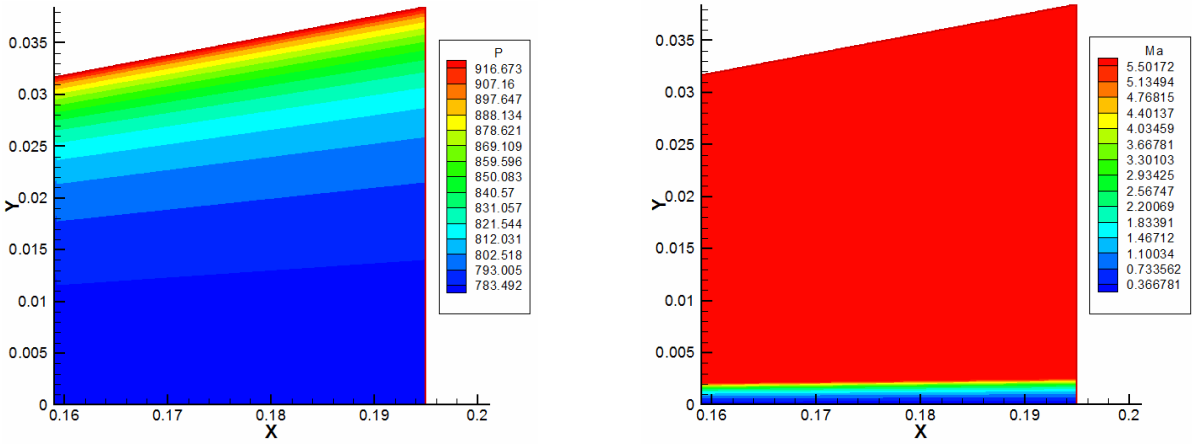

Figure 6. *Contours for steady Mach 5.92 flow over a flat plate zone 8 without the roughness (a), pressures (b),velocity.*

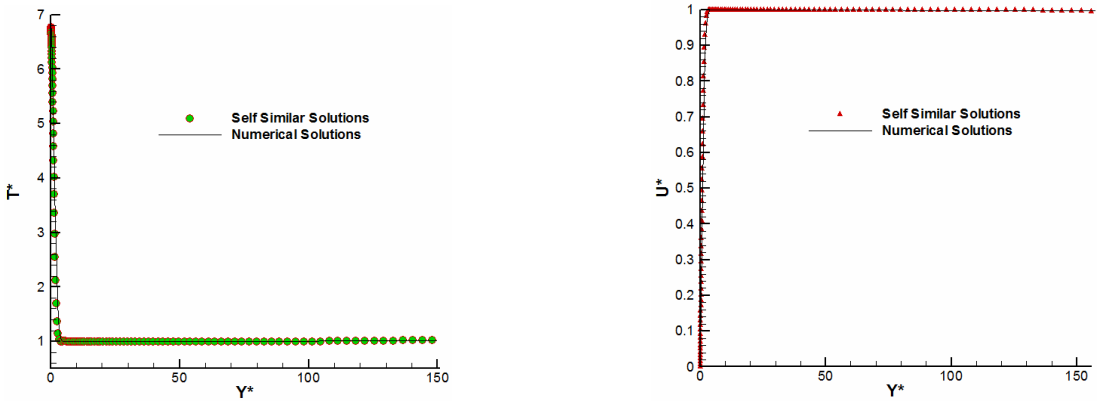

Figure 7. *Along a wall-normal grid line which is originated from a point located at* $x = 0.1676m$ *on the plate surface. (a), temperature (b),velocity in y direction profile.*

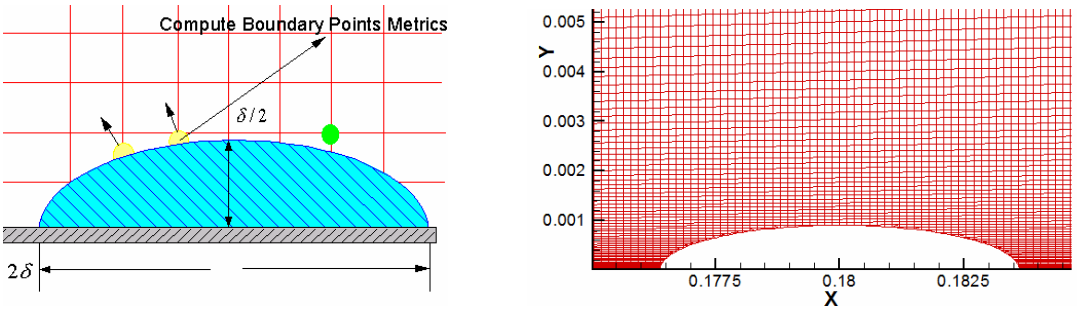

Figure 8. *(a),General roughness geometry (b), Cartesian grids generation.*

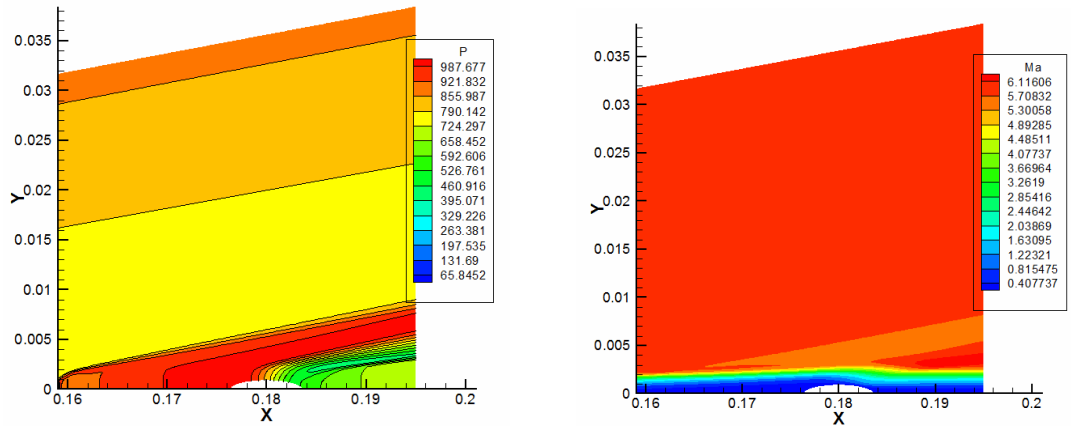

Figure 9. *Contours for steady Mach 5.92 flow over a flat-plate zone 8 with surface roughness* $h/\delta = 1/2$ *(a), pressures (b),Mach number.*

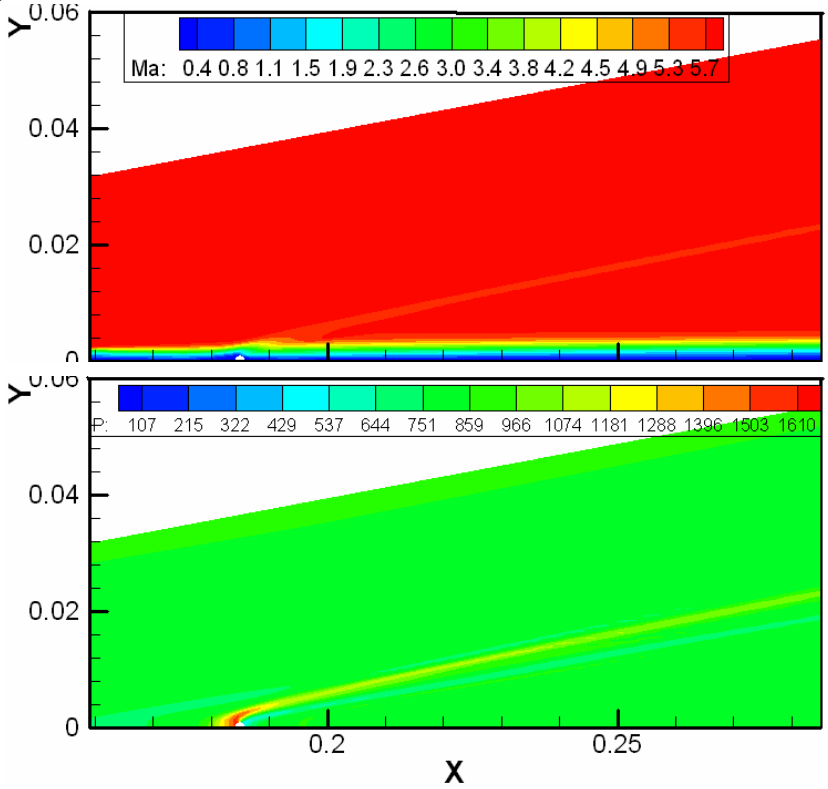

Figure 10. *Contours for steady Mach 5.92 flow over a flat-plate at zone 8-zone 10 with surface roughness* $h/\delta = 1/2$ *(a),Mach number (b),pressure.*

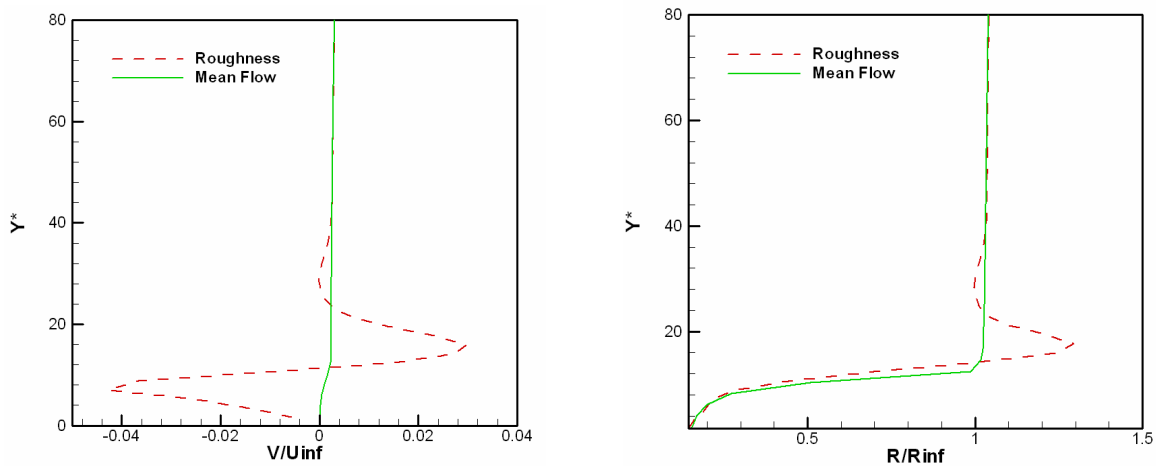

Figure 11. *Along a wall-normal grid line at $x = 0.188m$ on the plate surface (a), horizontal velocity (b), density profile for flow with and without roughness.*

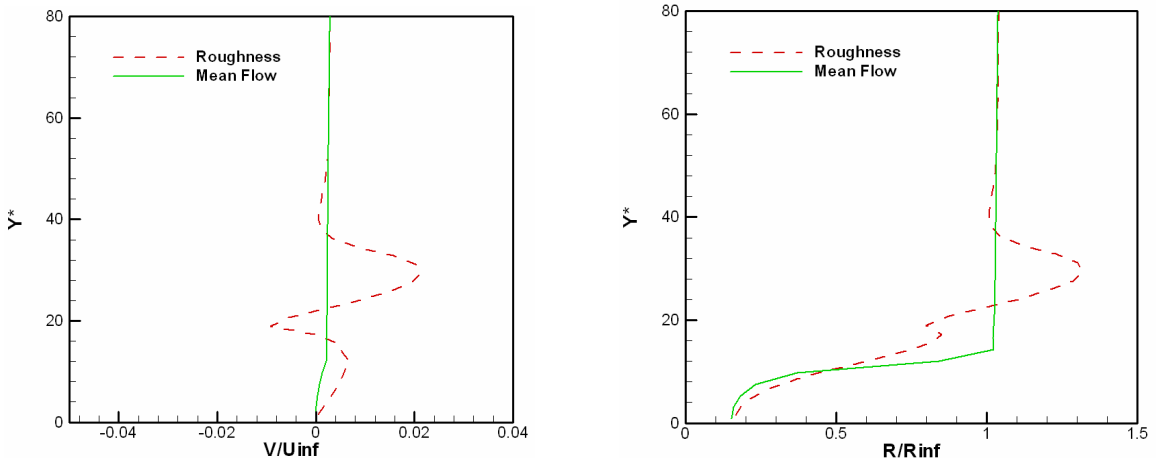

Figure 12. *Along a wall-normal grid line at $x = 0.200m$ on the plate surface (a) spanwise velocity (b), density profile for flow with and without roughness.*

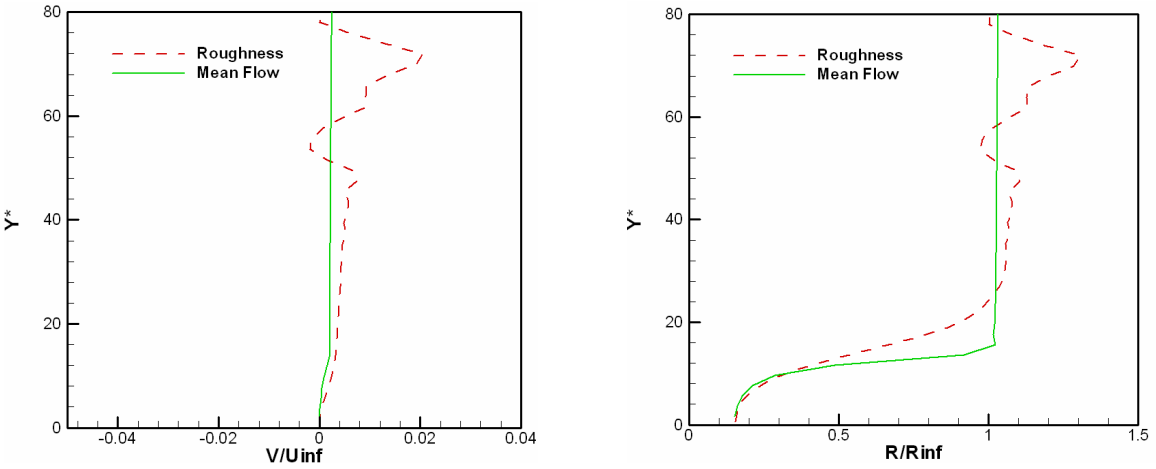

Figure 13. *Along a wall-normal grid line at $x = 0.240m$ on the plate surface (a), horizontal velocity (b), density profile for flow with and without roughness.*

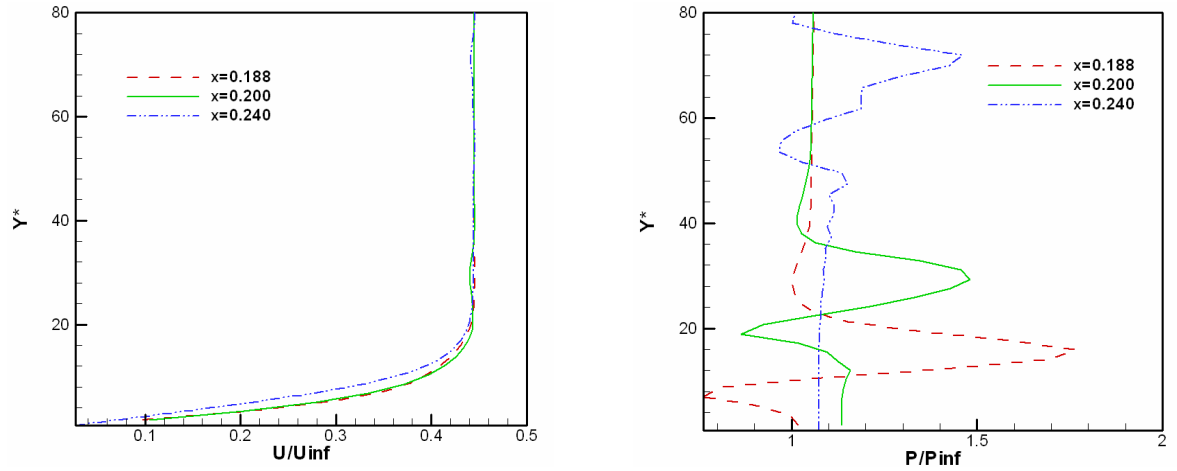

Figure 14. *The evolution of disturbance profile at different locations (a), streamwise velocity (b), pressure.*

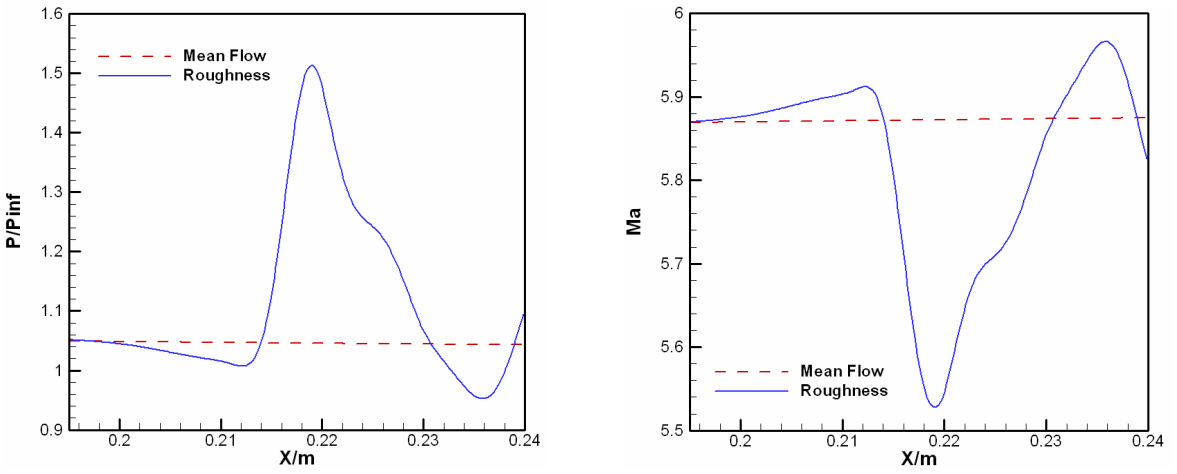

Figure 15. *Along a vertical grid line at fixed* $y = 0.010m$ *the profile of (a) pressure (b), Mach number for flow with and without roughness.*

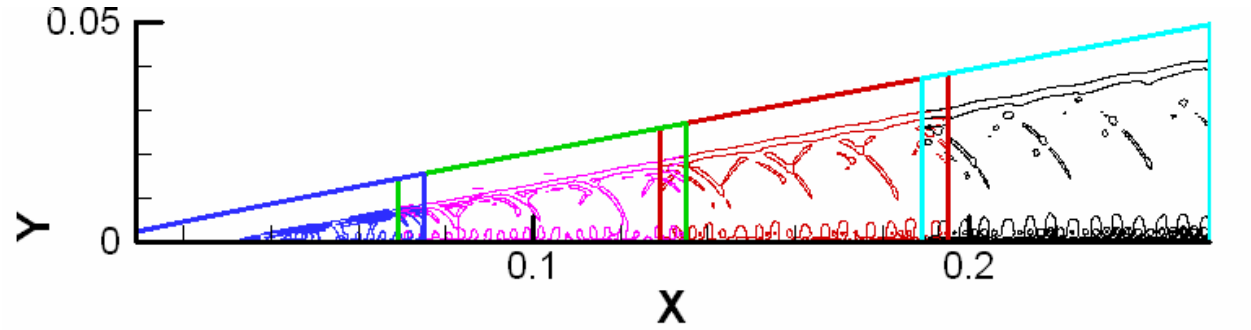

Figure 16. *Pressure disturbance contour for unsteady flow field with external disturbance from zone 3 to zone 10.*

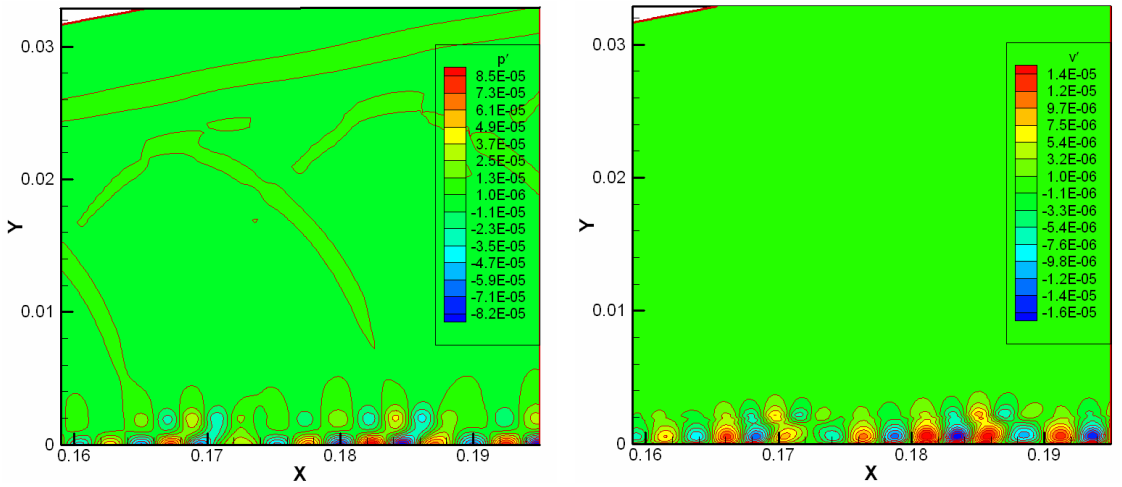

Figure 17. *Contours for unsteady Mach 5.92 flow over a flat plate zone 8 without the roughness (a), pressures (b),horizontal velocity.*

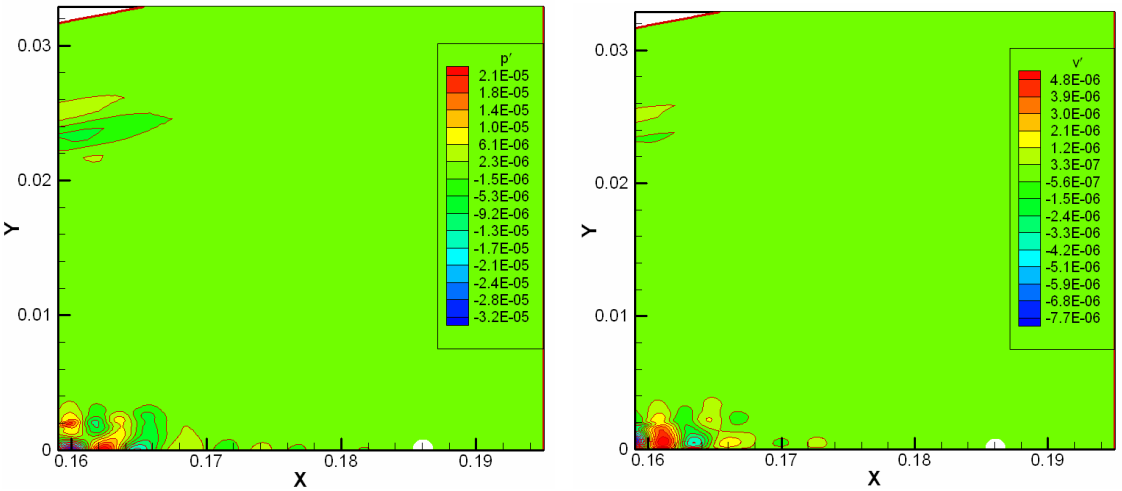

Figure 18. *Contours for unsteady Mach 5.92 flow over a flat plate zone 8 with surface roughness (a), pressures (b),horizontal velocity.*

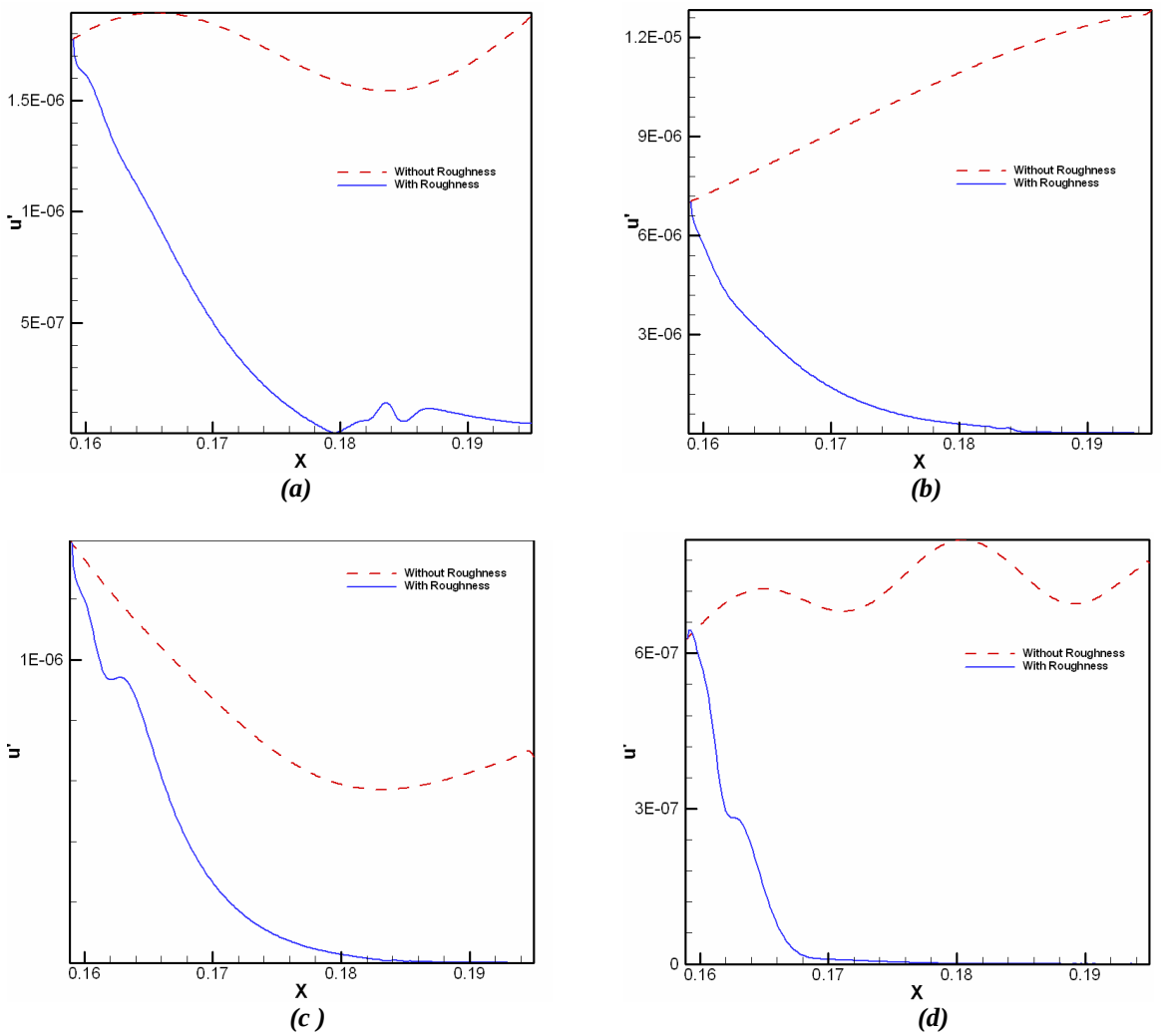

Figure 19. *Maximum magnitude of streamwise velocity disturbance with different frequency after FFT for Mach 5.92 flow over flat-plate at zone 8 (a),n=2 (b), n=3 (c), n=4 (d), n=5.*